Experimental Study on the Small-strain Stiffness and the Damping Properties of Strong Structural Clay

Experimental Study on the Small-strain Stiffness and the Damping Properties of Strong Structural Clay

Mingyuan Wang, Zhigang Shan, Miaojun Sun and Kuanjun Wang

Power China Huadong Engineering Corporation Limited, Hangzhou, Zhejiang, 310012, China

Corresponding author's e-mail: 409976046@qq.com

Abstract The small strain parameters of soil are important indexes for correct evaluation of the soil deformation. Based on the Stokoe resonant column system, the small strain dynamic characteristics of Zhanjiang strong structured clay under different consolidation stresses are investigated, including the dynamic shear modulus and damping ratio. Results show that under the same stress level, the maximum dynamic shear modulus of undisturbed soil is slightly larger than that of the remolded, and both of them decrease with the increase of shear strain. And the higher stress level is, the higher the maximum dynamic shear modulus would be, and the more significant the attenuation would be. As the shear strain increases to a certain extent, the damping ratio of the undisturbed soil increases sharply, but that of the remolded increases slowly. The maximum dynamic shear modulus of undisturbed soil shows a singular feature that it increases at the beginning and then decreases with the increase of effective confining pressure; and the inflection point corresponding to the effective confining pressure is larger than the structural yield stress of soil. The maximum dynamic shear modulus of the undisturbed soil is not only affected by the positive effect of the consolidation pressure and void ratio, but also affected by the negative effect of the structural damage induced by the stress level.

1. Introduction

The small-strain parameters of soil are important metrics for evaluating their deformations. Burland noted that soil strains surrounding underground structures (e.g., foundation pits, tunnels and bases) range from 0.01% to 0.1% in most areas except for a few that contain plastic zones [1]. Atkinson et al. classified the soil strain into three types, namely, the micro-strain (≤0.001%), the small strain (0.001%–0.1%) and the large strain (>0.1%) [2]. Extensive engineering field measurements demonstrate that a considerable number of soils surrounding geotechnical engineering structures are in the small-strain condition under working loads. In recent years, extensive studies have been conducted to examine the small-strain behaviour of soil through high-precision laboratory and in situ tests, and the stiffness of soil has been found to be highly nonlinear under the condition of the small strain [3-7].

Generally, study on the small-strain properties of soil is focused on two areas: the initial modulus or maximum dynamic shear modulus G_{max} at the small strain and the variation trend of soil stiffness within the small-strain range. Mandy factors would affect the G_{max} of soil, such as the strain amplitude, stress level and void ratio. The Hardin equation can be used to calculate the G_{max} of soil at the small strain and reflect the effect of the over-consolidation ratio, void ratio and effective stress on G_{max} [8]. In engineering practice, G_{max} of a soil at the small strain is generally estimated based on its physical parameters and stress state using an empirical equation. The decrease of stiffness with increasing

strain is described based on the dynamic shear moduli G corresponding to various shear strains γ. A critical shear strain $\gamma_{0.7}$ is often used to quantify the extent of decrease in the small-strain stiffness of soil. The Hardin-Drnevich equation can depict the whole curve of the decrease of G with γ [9].

Structured clays are widely distributed, and their strength and deformation are both restricted by their strong structure properties. The structure of a soil is closely related to its stress state [10-11]. To date, effects of the structure on G at various stress levels have been rarely investigated. Park statistically analyzed the existing results and summarized the initial G–confining pressure σ relationship for various soils as a power function relationship [12]. For most sandy, silty and soft soils, G increases with increasing consolidation pressure (i.e., σ). However, the mechanical properties of structured soils differ from those of normal soils, and their mechanical behaviours differ significantly when they are subjected to a lower or higher pressure than the structural yield stress. Whether the variation trend of G with σ remains unchanged after the point of structure yielding stress deserves further in-depth investigation. In addition, structural damages in the structured soil evolve with the increase of average stress. In characterizing the G_{max} of a soil at the small strain, the Hardin equation only takes into consideration the increase of G_{max} caused by the increase in effective stress but neglects the effect of the structural damage. Hence, the applicability of the Hardin equation to calculate G_{max} for structured soils at the small strain remains unclear.

In view of the above mentioned limitations, in this study, resonant column tests are performed on undisturbed and remoulded specimens of strong structured clay at various σ levels to investigate the variation law of its dynamic parameters at the small strain. Through comparison, the G and damping ratio D of the structured clay at various σ levels are analyzed. In addition, the correlation between the shear strength of the structured clay and variation of its stiffness is discussed.

2. Test soil sample, equipment and method

2.1. Test soil sample

A soil sample was collected from a sedimentation layer at a depth ranging from 7.0 m to 10.0 m in a coastal zone of Zhanjiang, in China. The soil layer contained horizontal thin beddings with intermediate visible sand grains. Preliminary mechanical tests revealed that the undisturbed soil sample had an unconfined compressive strength of 150 kPa, a structural yield strength as high as 400–600 kPa and a sensitivity of 5–7, which belongs to a typical high-sensitivity and strong-structured soil.

2.2. Test equipment

The resonant column test can measure the dynamic deformation properties of soil within a strain range of 10^{-6}–10^{-3} and is considered the most reliable laboratory method for measuring the soil small-strain parameters. In this study, a fixed-free Stokoe resonant column apparatus (RCA) (GDS Instruments, UK) was used. The GDS RCA consists of a drive system, a monitoring system, a drainage system and a pressure chamber, as shown in Figure 1. The GDS RCA applies vibration excitation to the top of a cylindrical solid soil specimen, generates a torsional or longitudinal excitation via the electromagnetic drive system, determines the transmitted wave velocity and the damping of the soil specimen by measuring its motion at its free end, and calculates G based on the measured shear velocity and specimen density.

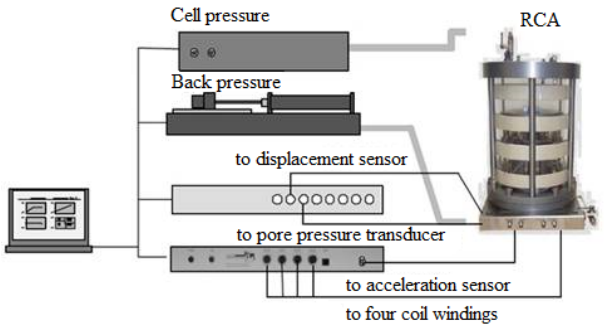

Figure 1. The GDS RCA test system.

Figure 2 shows the drive system of the Stokoe RCA. The drive system consists of a four-arm rotor and a support column. There is a permanent magnet at the bottom of each arm of the four-arm rotor. The support column is used to fix four pairs of coils. A sinusoidal voltage is first applied to the electromagnetic coils, which then generates a driving force on the driving head and thereby applies a torsional force on the specimen. The frequency and amplitude of the excitation applied to the specimen can be varied by adjusting the frequency and amplitude of the current applied to the electromagnetic coils. When the driving frequency equals to the natural (resonant) frequency of the specimen, the specimen reaches its maximum vibration amplitude, which can be monitored by the acceleration sensor. The frequency corresponding to the maximum vibration amplitude of the specimen is the natural (resonant) frequency, based on which the G of the specimen can be calculated.

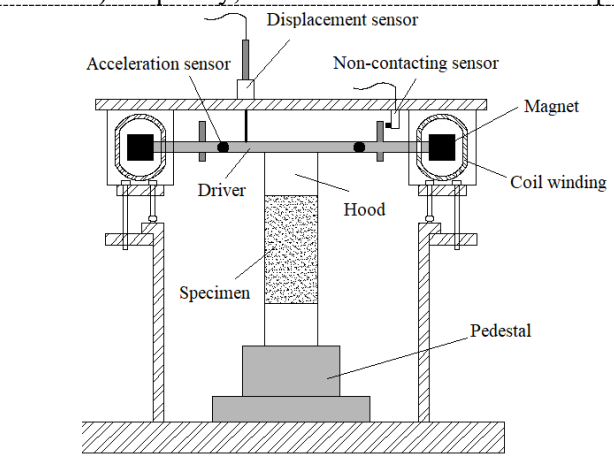

Figure 2. Structural diagram of the drive system of the RCA.

The fundamental equation for the Stokoe RCA is as follows:

$$\frac{I}{I_0} = \beta \tan \beta \tag{1}$$

where I is the rotational inertia of the soil specimen, and I_0 is the rotational inertia of the drive system of the resonant column. However, due to the complex geometric shape of the drive system, an accurate value of I_0 cannot be mathematically determined. Generally, I_0 is determined through an empirical value table.

The shear wave velocity V_s can be calculated using the following equation:

$$V_s = \frac{2\pi fH}{\beta} \tag{2}$$

G can be determined based on V_s:

$$G = \rho V_s^2 = \rho\left(\frac{2\pi fH}{\beta}\right)^2 \tag{3}$$

where ρ is the mass density of the soil specimen, G is the dynamic shear modulus of the soil specimen, f is the resonant frequency, H is the height of the soil specimen, and β is the eigenvalue of the torsional vibration frequency equation.

The viscous damping ratio D of soil specimen measured by the resonant column is obtained based on a free vibration damping curve, which is measured by the acceleration sensor installed on the drive plate of the resonant column. After the torsional (flexural) resonance test, the resonant frequency of the specimen is obtained. Subsequently, a damping test is conducted, and the resonant frequency automatically provides the damping test parameter. A sinusoidal wave is applied to the soil specimen; then, the excitation is terminated, and the free vibration of the soil specimen is measured. The decrement δ in the logarithmic expression of the damping curve can be calculated based on the continuous cyclic vibration amplitude ratio: δ is calculated by plotting a curve depicting the relationship between the peak vibration amplitude and number of cycles. Theoretically, this curve is expected to be a straight line with a slope of δ.

The viscous damping ratio D of the soil specimen is then calculated based on δ:

$$D = \sqrt{\frac{\delta^2}{4\pi^2 + \delta^2}} \tag{4}$$

2.3. Test method

Undisturbed and remoulded specimens of Zhanjiang strong-structure clay (ZSSC) were each examined by the resonant column test. Each specimen was subjected to a multi-level consolidation (isotropic consolidation) test. After each specimen was drained and consolidated at a certain pressure level, the amount of consolidation settlement and amount of drainage were measured. Subsequently, the vibration stress was increased incrementally, and the vibration frequency of the specimen and the corresponding shear stress were measured. The power was then cut off, the vibration damping curve of the specimen was measured, and the volumetric change and void ratio of the specimen were calculated. In addition, G for the specimen was calculated based on equation (3). The specimen was then subjected to the next level of consolidation until it had been tested all the σ levels.

A high-quality undisturbed ZSSC sample was collected using a fixed piston thin-walled sampler. A remoulded specimen was prepared by kneading. The structure of a piece of undisturbed ZSSC sample was destructively converted into a sludge form, and then was remoulded and shaped. Each specimen had a diameter of 50 mm and a height of 100 mm. Each specimen was saturated using two techniques successively (namely, vacuum saturation and back-pressure saturation) to allow its degree of saturation to reach above 98%, after which the specimen was tested. The following effective σ levels were used in the test: 100, 200, 400, 600 and 800 kPa.

3. Test results and analysis

3.1. The variation of dynamic parameters at the small strain

Figure 3 shows the G–γ curves of ZSSC at various σ levels. G gradually decreases as γ increases. When γ is relatively small, G decreases slowly as γ increases. However, after γ increases to a certain

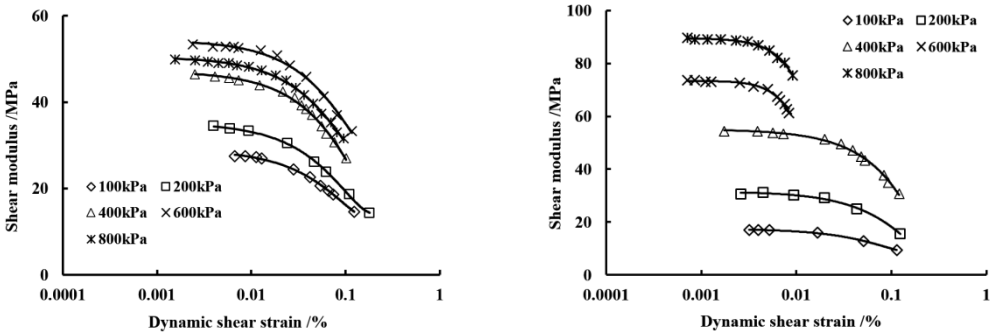

(a) G–γ curve of the undisturbed specimen (b) G–γ curve of the remoulded specimen

Figure 3. G–γ curves of ZSSC.

extent, G starts to decrease rapidly as γ increases. A comparison of the test curves of the undisturbed and remoulded specimens at various σ levels shows that under the same excitation voltage, a higher σ corresponds to a smaller measured minimum γ, and more significant decreases in G with the increase of γ. In addition, an inconsistency of the G variation can also be observed between the undisturbed and remoulded specimens with changing σ. For the remoulded specimen, G–γ curve gradually goes up as σ increases, and it is varied monotonically. For the undisturbed specimen, G–γ curve does not change monotonically but instead first goes up and then down with the increase of σ. The notable phenomenon can be observed in Figure 4(a).

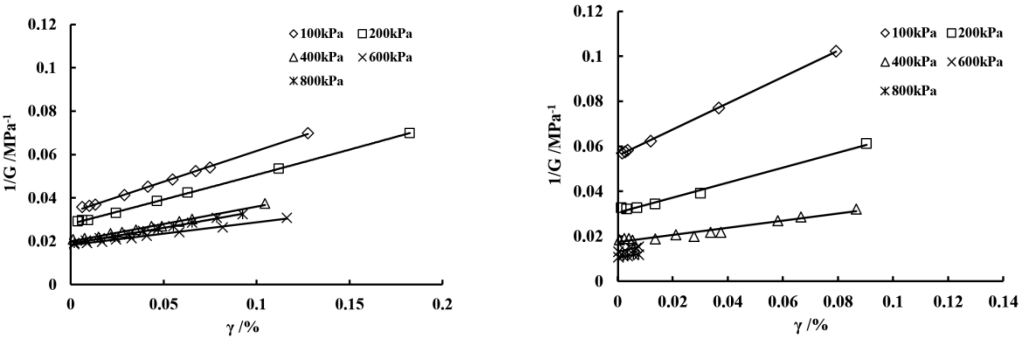

(a) G–γ curve of the undisturbed specimen (b) G–γ curve of the remoulded specimen

Figure 4. 1/G-γ relationship of ZSSC.

Here, the Hardin-Drnevich [9] hyperbolic model is used to describe the relationship between the measured dynamic shear stress τ and γ amplitude:

$$\tau = \frac{\gamma}{a + b\gamma} \tag{5}$$

where a and b are test parameters. Furthermore, G for the soil can be expressed as follows:

$$G = \frac{1}{a + b\gamma} \tag{6}$$

Based on equation (6), a straight-line relationship exists between 1/G and γ. By fitting the curves, as shown in Figure 4, G_{max} values at various σ levels can be obtained (i.e., $G_{max} = 1/a$).

The test data of G for the undisturbed specimen were normalized relative to G_{max}, as shown in Figure 5(a). In addition, the normalized results for the G/G_{max}–γ curves of soils obtained from other

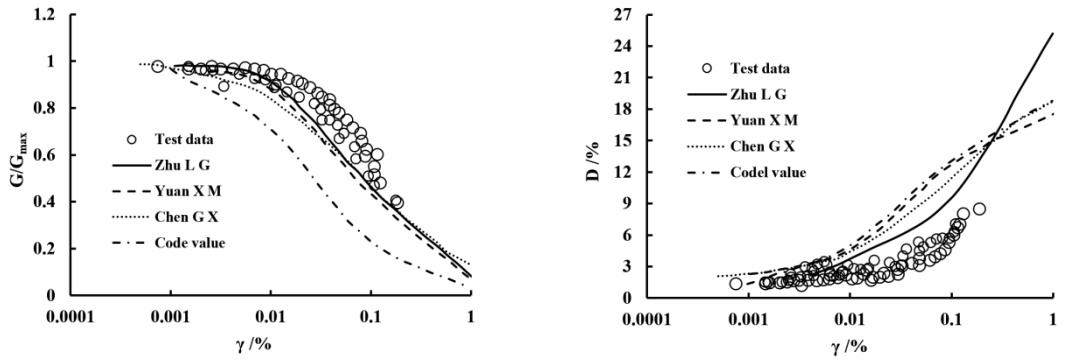

(a) G/G_{max}-γ comparison curves (b) D–γ comparison curves

Figure 5. G/G_{max}-γ and D-γ comparison curves of the undisturbed ZSSC.

studies (e.g., by Zhu et al., Vucetic et al., Yuan et al. and Chen et al. [13-15]) are plotted in Figure 5(a) for comparison to elucidate the differences in dynamic properties between ZSSC and other clays. Similarly, the relation curves between the damping ratio D and the shear strain γ for the undisturbed specimen were conducted and shown in Figure 5(b). In Figure 5(a), the test values of ZSSC at various σ levels are distributed in a relatively narrow zone, which is relatively close to the distribution pattern of values obtained by Zhu et al., and the determination of G/G_{max} is essentially independent of the stress state of the clay. Moreover, the results of Zhu et al., Vucetic et al., Yuan et al. and Chen et al. are basically consistent with the outcomes of this study; i.e., all the values are significantly higher than those from the earthquake resistant code. Thus, it is too conservative an approach to select dynamic parameters based on the specification.

In Figure 5(b), the test values of D of ZSSC at a strain smaller than 10^{-4} are mainly concentrated near the values of Chen et al. and Yuan et al., and start to become dispersed when the strain exceeds 10^{-4}. The test values of D are lower than those from the earthquake resistant code. And the results for D are more dispersed than those for G/G_{max}, which is consistent with the current understanding of damping.

Figure 6 shows the D–γ curves of the undisturbed and remoulded specimens at various σ levels. As demonstrated in Figure 6(a), for the undisturbed specimen, D increases as γ increases at each σ level and increases sharply after γ increases to a certain extent. Compared with Figure 3(a), it is found that the stage of G decreasing rapidly corresponds to the stage of D increasing rapidly. By contrast, the D–γ curves of the remoulded specimen increase relatively smooth with the increase of γ (Figure 6(b)).

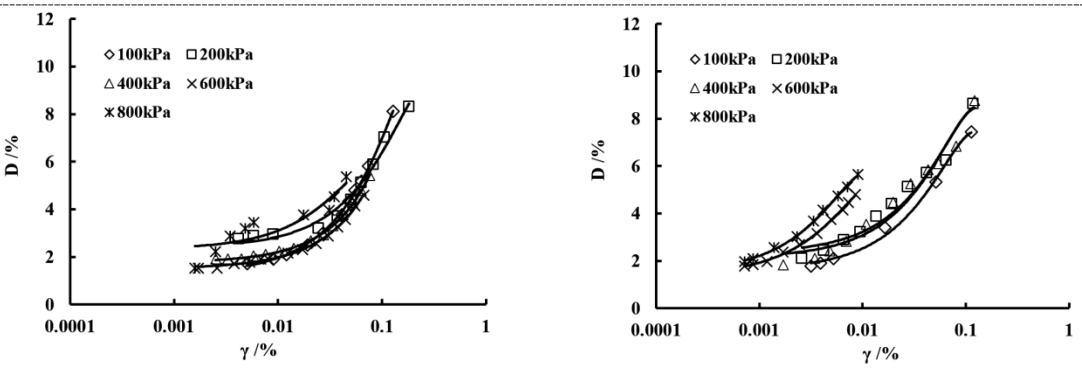

(a) D-γ curve of the undisturbed specimen (b) D-γ curve of the remoulded specimen

Figure 6. D–γ curves of ZSSC.

3.2. Description of G and D

Based on the Mohr–Coulomb criterion and the Hardin-Drnevich hyperbolic nonlinear stress–strain model, the following G equation was proposed [9]:

$$G(\gamma) = \mathrm{G}_{\max}(1 - f(\gamma)) \tag{7}$$

$$f(\gamma) = \frac{\gamma / \gamma_{ref}}{1 + \gamma / \gamma_{ref}} \tag{8}$$

where γ_{ref} is the reference shear strain.

For the equation (7), all of parameters have their definite physical meanings. However, it is not fit for different soil types due to the relatively small number of fitting parameters. Several researchers have revised the Hardin–Drnevich model by using a three-parameter Davidenkov model to correct the f(γ) [16]:

$$f(\gamma) = \left(\frac{(\gamma / \gamma_0)^{2B}}{1 + (\gamma / \gamma_0)^{2B}} \right)^{A} \tag{9}$$

where γ_0, A and B are fitting parameters related to the soil type (γ_0 is no longer a reference shear strain with a well-defined physical meaning).

The Davidenkov stress–strain relationship model can be expressed as follows:

$$\tau(\gamma) = G(\gamma)\gamma \left(1 - \left(\frac{(\gamma / \gamma_0)^{2B}}{1 + (\gamma / \gamma_0)^{2B}} \right)^{A} \right) \tag{10}$$

Based on G, Hardin & Drnevich proposed the following empirical equation for calculating D:

$$D = D_{\max}\left(1 - \frac{G}{G_{\max}}\right) \tag{11}$$

where D_{max} is the maximum damping ratio (D = D_{max} when G = 0).

In engineering practice, because the fit of D to the test results is not ideal, another empirical equation is often used to describe the D–γ relationship [16]:

$$D = D_{\min} + D_{\max}\left(1 - \frac{G}{G_{\max}}\right)^{n} \tag{12}$$

where D_{min} is the minimum damping ratio, which is the basic damping ratio of the soil and is related to the properties and consolidation state of the soil, and n is a fitting parameter related to soil type.

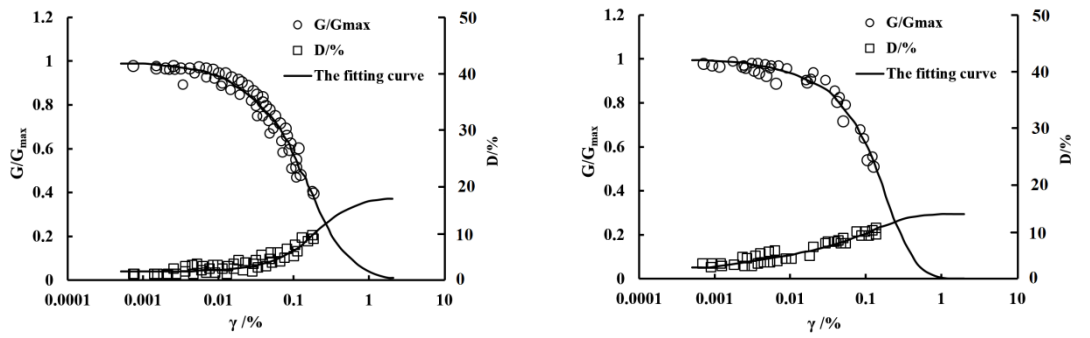

(a) The undisturbed specimen (b) The remoulded specimen

Figure 7. G/G_{max}–γ and D–γ curves of ZSSC.

Figure 7 shows the distribution of the test values of the undisturbed and remoulded specimens at each σ level in addition to the model-fitted curves. The test values of the undisturbed and remoulded specimens are relatively insignificantly dispersed and distributed in a relatively narrow zone. The Hartin–Davidenkov model and the empirical D–γ equation (equation (12)) can satisfactorily fit the variation of G/G_{max} and D with the change of γ.

4. Test Correlation between the stiffness and strength of ZSSC

Figure 8 shows the G_{max}–σ curves of ZSSC obtained from the tests. G_{max} of the remoulded specimen increases with the increasing of σ, which shows a feature of monotonicity. Through comparison, a peculiar phenomenon is observed — G_{max} of the undisturbed specimen first increases and then decreases as σ increases. The value of σ corresponding to the inflection point is greater than the structural yield stress of soil, suggesting the occurrence of hysteresis. A comparison of the undisturbed and remoulded specimens under the same consolidation conditions shows that the G of the undisturbed specimen is slightly higher than that of the remoulded specimen at relatively low σ levels, but becomes lower than that of the remoulded specimen as σ increases. As σ reaches 600 kPa, the G_{max} of the undisturbed specimen starts to decrease, its skeleton gradually becomes fractured due to compression, and its stiffness gradually decreases. At the post-structural yield stage, σ increases until the structure of specimen collapses, at which time the specimen completely loses its structure.

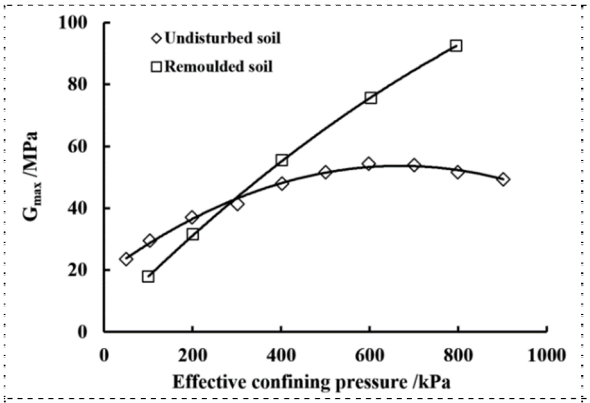

Figure 8. G_{max}–σ curves of ZSSC.

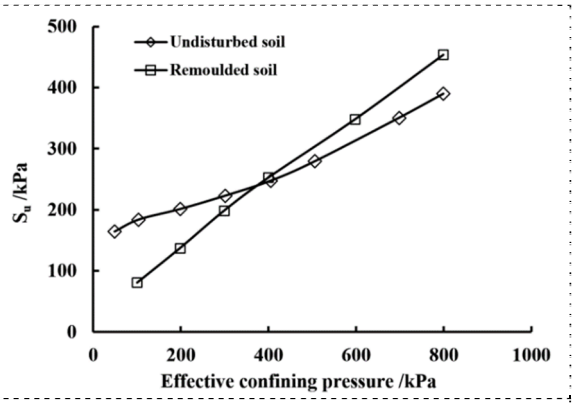

Figure 9. S_u–σ curves of ZSSC.

Figure 9 shows the undrained shear strength S_u–σ curves of the undisturbed and remoulded specimens under the static load. The S_u–σ curve of the undisturbed specimen has a notable inflection point, whereas the S_u–σ curve of the remoulded specimen is a straight line. For the undisturbed specimen, when σ is lower than the structural yield stress of the soil, its structural strength plays the dominant role, and the effects of consolidation and compaction are insignificant; consequently, its deformation is insignificant. When σ exceeds the structural yield stress, its structural strength gradually decreases to zero, and the cementation between particles decreases; consequently, the structure is significantly compacted, which is reflected by the inflection point of the S_u–σ curve.

The resonant column and triaxial undrained consolidation test results both demonstrate that under low effective confining pressures, the G_{max} and peak Su of the undisturbed specimen are both higher than those of the remoulded specimen; however, after the pressure exceeds the structural yield stress of the soil, due to consolidation, the remoulded specimen has a relatively high G and τ, which is reflected by its relatively high stiffness and strength.

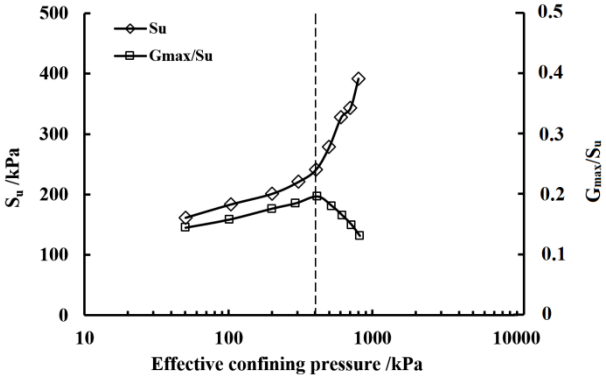

Figure 10. Variation in the G_{max}/S_u ratio of ZSSC with σ.

Figure 10 shows the variation in the G_{max}/S_u ratio of ZSSC with the change of σ. As demonstrated in Figure 10, the G_{max}/S_u ratio displays notable multi-stage characteristics as σ increases. The clay sustains relatively small structural damage at low σ levels. As σ increases, both the strength and stiffness of the clay increase. The G_{max}/S_u ratio of the undisturbed specimen also increases as σ increases. An inflection point appears on the G_{max}/S_u–σ curve of the undisturbed specimen at σ value of 400 kPa. After σ reaches 400 kPa, the G of the undisturbed specimen still increases as σ increases, but at a much slower rate than S_u, resulting in a decrease in the G_{max}/S_u ratio. As σ further increases, the undisturbed specimen sustains progressive structural damage, and its strength gradually approaches that of the remoulded specimen. In addition, as σ increases, the S_u of the undisturbed specimen starts to increase at an increasing rate, whereas the G_{max}/S_u ratio decreases significantly. This result suggests that for the undisturbed strong –structured soil, the degree of attenuation of its stiffness caused by the structural damage is greater than that of its shear strength.

5. Discussions

A peculiar phenomenon is observed from the G_{max}–σ curve of the undisturbed ZSSC specimen—G_{max} first increases and then decreases with the increasing σ. The σ corresponding to inflection point is higher than the structural yield stress of soil. Only the stress corresponding to the inflection point on G_{max}/S_u–σ curve or G_{max}–σ curve normalized by the void ratio function is almost equal to the structural yield stress of soil. If the initial consolidation pressure falls within the range between the structural yield stress and the pressure corresponding to the inflection point of the G_{max}–σ curve, G increases to a smaller extent than S_u as σ increases from the beginning.

Compressive hardening of soil is one of its important features during compression, i.e, soil modulus increases with its increasing density. For the structured clay, this property would be significant difference. Based on the influence mechanism of compressive hardening and structure on the soil strength and stiffness, it is concluded that G_{max} of the undisturbed ZSSC specimen is not only positively affected by σ and the void ratio function, but also negatively affected by the structural damage induced by σ. When σ is lower than the structural yield stress of soil, the positive effects play the dominant role; when σ is higher than the structural yield stress, the positive effects are less significant than the negative weakening effects of the structural damage of the undisturbed specimen on G. In addition, the structural damage of the undisturbed specimen caused by increasing σ is progressive and irrecoverable, and affects G and the shear strength Su to varying degrees at different stages.

6. Conclusions

This study investigated the small-strain parameters— G and D of undisturbed and remoulded ZSSC specimens with the resonant column tests. The conclusions derived from this study are summarized as follows:

1) At the same σ level, the G_{max} of the undisturbed specimen was slightly higher than that of the remoulded specimen. The G of the undisturbed and remoulded specimens both decreased as γ increased. A higher σ corresponded to a higher G_{max}, and a more significant decrease in G_{max} with the increase of γ.

2) The D of both the undisturbed and remoulded specimens increased as γ increased. However, after γ increased to a certain extent, the D of the undisturbed specimen started to increase sharply, whereas the D of the remoulded specimen increased smoothly.

3) A peculiar phenomenon was observed for the G_{max} of the undisturbed specimen—the value first increased and then decreased as σ increased. In addition, σ corresponding to the inflection point of the G_{max}–σ curve of the undisturbed specimen was higher than the structural yield stress. The G_{max} of the undisturbed specimen was positively affected by σ and the void ratio, and negatively affected by σ-induced structural damage.

4) The structural damage of the clay caused by σ resulted in a more significant decrease in G_{max} than in S_u.

References

[1] Burland J B. (1989) The ninth laurits bjerrum memorial lecture: Small is beautiful-the stiffness of soils at small strains. Canadian Geotechnical Journal, 26(4): 499-516.
[2] Atkinson J H, Stallfors G. (1991) Experimental determination of stress-strain-time characteristics in laboratory and in situ tests. General Report to Session 1 of Proceedings of the 10th European Conference on Soil Mechanics and Foundation Engineering, Florenze, pp. 915-956.
[3] Mair R J. (1993) Developments in geotechnical engineering research: Application to tunnels and deep excavations. Proceedings of the Institution of Civil Engineers, London, pp. 915-956.
[4] Kung T. C. (2007) Equipment and testing procedures for small strain triaxial tests. Journal of the Chinese Institute of Engineers, 30(4): 579–591.
[5] Benz T, Vermeer P A, Schwab R. (2009) A small-strain overlay model. International Journal for Numerical and Analytical Methods in Geomechanics, 33(1): 25-44.
[6] Zhang J, Wang W D, Xu Z H, Li Q. (2017) Laboratory test of small-strain characteristics of typical Shanghai cohesive soils. Rock and Soil Mechanics, 38(12): 3590-3595.
[7] Gu X Q, Lu L T, Li X W, Ju S W. (2018) Experimental study of small strain stiffness properties of soil. Journal of Tongji University, 46(3): 312-317.
[8] Hardin B O, Black W L. (1968) Vibration modulus of normally consolidated clay. Journal of Soil Mechanics and Foundations Division, ASCE, 94(2): 453-469.
[9] Hardin B O, Drnevich V P. (1972) Shear modulus and damping in soils: Measurement and parameter effect. Journal of the Soil Mechanics and Foundation Division, ASCE, 98(6): 603-624.
[10] Shen J H, Wang R, Zheng Y, Han J Z, et al. (2013) Research on regional microstructure characteristics of structural clay of Zhanjiang formation. Rock and Soil Mechanics, 34(7): 1931-1936.
[11] Zhang L. (2010) Zhanjiang formation of Quaternary clay engineering characteristics, Mining Technology, 10(1): 24 -25.
[12] Park D. (1998) Evaluation of dynamic soil properties: strain amplitude effects on shear modulus and damping ratio, Cornell University.
[13] Chen G X, Xie J F, Zhang K X. (1995) The empirical evaluation of soil moduli and damping ratio for dynamic analysis, Earthquake Engineering and Engineering Vibration, 15(1): 73-84.
[14] Yuan X M, Sun Y, Sun J, Meng S J, et al. (2000) Laboratory experimental study on dynamic shear modulus ratio and damping ratio of soils. Earthquake Engineering and Engineering Vibration, 15(1): 73-84.

[15] Sun J, Yuan X M, Sun Y. (2004) Reasonability comparison between recommended and code values of dynamic shear modulus and damping ratio of soils. Earthquake Engineering and Engineering Vibration, 24(2): 125-133.
[16] Jia P F, Kong L W, Wang Y, Yang A W. (2013) Nonlinear characteristics and determinate method of elastic stiffness for soils due to low-amplitude small-strain vibrations. Rock and Soil Mechanics, 34(11): 3145-3151.